Science in China Series G: Physics, Mechanics & Astronomy

© 2009 SCIENCE IN CHINA PRESS

Springer

www.scichina.com
phys.scichina.com
www.springerlink.com

Tracking moving magnetic features in the photosphere

LI XiaoBo[1,2†], BÜCHNER Jörg[2] & ZHANG HongQi[1]

[1] Key Laboratory of Solar Activity, National Astronomical Observatories, Beijing 100012, China;

[2] Max-Planck-Institut für Sonnensystemforschung, Max-Planck-Str.2, 37191, Katlenburg-Lindau, Germany

This research aims for an objective identification, tracking, and a statistical analysis of the Moving Magnetic Features (MMFs) around sunspots using SOHO/MDI high-resolution magnetograms. To this end, we develop a computerized tracking program and study the motion and magnetism of the outflows of MMFs around 26 sunspots. Our method locates 4-27 MMFs per hour, with higher counts for large sunspots. We differentiate MMFs into type α that have a polarity opposite to the parent sunspots, and type β that share the sunspot's polarity. These sunspots' MMF subsets exhibit a wide range of central tendencies which have distinctive correlations with the sunspots. In general, α-MMFs emerge farther from the sunspot, carry less flux, and move faster than β-MMFs. The typical α/β-MMFs emerge at 2.2 – 8.1/0.1 – 3.2 Mm outside the penumbra limb, with lifetimes of 1.1 – 3.1/1.3 – 2.0 h. They are 1.1 – 6.6/1.4 – 3.6 Mm^2 in area and carry 1.4 – 12.5/4.8 – 11.4 $\times 10^{18}$ Mx of flux. They travel a distance of 2.7 – 5.9/2.8 – 3.6 Mm with the speed of 0.5 – 0.9/0.4 – 0.7 km/s. Compared to the α-MMFs produced by large sunspots, those of small spots are smaller. They emerge closer to sunspot, move farther, live longer, and carry less flux. β-MMFs show much less correlation with the sunspots. The flux outflow carried by the MMFs ranges from 0.2 to 8.3 $\times$ 10^{19}Mx$\cdot$ h^{-1} and does not show obvious correlation with the sunspots' evolution. The frequency distributions of the MMFs' distance traveled, area, and flux are exponential. This suggests the existence of numerous small, weak, and short-timescale magnetic objects which might contribute to the sunspot flux outflow.

sun, activity, magnetic fields, photosphere, sunspots, moat, moving magnetic features

On magnetograms, small-scale Moving Magnetic Features (MMFs) of both the same and opposite to the sunspots' magnetic field are observed to originate near the penumbra boundary and stream almost radially outward within the moat at a speed about 1 km/s and finally disappear in the moat or merge into the surrounding network. This flux outflow plays an intricate role in the mass and magnetic energy flow around sunspots and contributes to the evolution of the sunspots. MMFs can be bipolar or unipolar. Observing MMFs requires consecutive, short time-cadence, and high

Received July 17, 2009; accepted August 18, 2009
doi: 10.1007/s11433-009-0245-4

†Corresponding author (email: xiaobo_li_naoc@yahoo.com)

Supported by the National Basic Research Program of China (Grant No. 2006CB806301), the National Natural Science Foundation of China (Grant Nos. 10611120338, 10473016, 10673016, 10733020, and 60673158), the Important Directional Project of Chinese Academy of Sciences (Grant No. KLCX2-YW-T04), the Astronomical Unite Foundation of China (Grant Nos. 10878016 and 10778723), and the Max-Planck Gesellschaft – Chinese Academy of Sciences Doctoral Program and the International Max-Planck Research School

Citation: Li X B, Büchner J, Zhang H Q. Tracking moving magnetic features in the photosphere. Sci China Ser G, 2009, 52(11): 1737-1748, doi: 10.1007/s11433-009-0245-4

spatial-resolution magnetograms.

Since Sheeley[1], Vrabec[2], and the Harveys[3] made the first discoveries four decades ago, detailed observations[4−24] have been carried out by ground-based and space observatories to study these "steady flow of bright points". The observed MMFs move with a range of speeds around 1 km/s. The mean lifetimes of MMFs range from 1 to 8 hours. Their paths in the moat are almost radially outward from the sunspot along the continuation of dark filaments. MMFs show a range of sizes 1–2″ and carry a flux of the order of 10^{19} Mx. The net flux outflow transported by a sunspot's MMFs is about 1–10×10^{19} Mx· h^{-1}. MMFs are found to be associated with the Evershed flows and Hα fibrils and interact with other magnetic elements in the moat or the surrounding network. They might be visible as bright areas in the upper photosphere and lower chromosphere. Shine[4] categorized MMFs according to their polarity and pairing. (a) Type I, magnetic bipoles, (b) Type II, unipolar with same polarity as the sunspot, and (c) Type III, unipolar with opposite polarity to the sunspot. There also have been reports[5−7] about inflowing MMFs. MMFs are considered to be the intersections of the photosphere and the tiny flux tubes detached from sunspots[3]. To describe MMFs' physical nature, theoretical and schematic interpretations (e.g. "Ω-loop", "U-loop", and "O-loop" models) have been proposed and discussed[3,5−17].

In recent years, the study of MMFs has been advanced by the development of computerized tracing methods[25−29] which has made possible the automatic and objective study of large MMF sample sets. Hagenaar's method[27] finds 4–24 MMFs per hour around the 8 sunspots studied. MMFs live for about 1 hour and travel a distance of 3.5 Mm with an average outflow velocity of 1.5–1.8 km/s. The MMFs have an average flux content 2.5×10^{18} Mx with the maximum value 6.1×10^{18} Mx. MMFs are found to transport a net flux out of a sunspot at a rate of 0.4–6.2×10^{19} Mx·h^{-1}.

In spite of the knowledge accumulated about the MMF's morphological properties, the very fundamental structure and configuration are still ambiguous. Many observational details remain elusive, such as their interactions with the upper and lower chromosphere. There are only sparse observations on the details about their formation, evolution, fragmentation, merging, and disappearance. MMFs exhibit a wide range of average values in previous observations and the relationship between MMFs' statistical character and the sunspots has not been well studied. So far, it is still not clear how much and in which way MMF flux outflow accounts for the decay of sunspots.

1 Data and method

1.1 Data

We investigate 26 sunspots with various radii (6−23 Mm), polarities, and in different developing phases (growing, stable, or decaying). Most of the sunspots are round and solitary. The data are the high-resolution longitudinal magnetograms of SOHO/MDI taken in the period of 2000 − 2004. The time cadence is 1 minute and the spacial resolution is 0.6″ $pixel^{-1}$. The selected sequences are consecutive and contain few ineligible images. Their time durations are long enough (5.5−18.1 h) to track MMFs. Their noise levels are about 20 Gauss. For most of the magnetogram sequences, we also prepare their corresponding MDI filtergram sequences. These filtergram series are recorded at wavelengths near the Ni I 6768 Å[30]. Their time duration, resolution and field-of-view are the same as those of the magnetogram series. They are used for the determination of the sunspot boundaries. If the filtergrams are not available on-line, magnetograms are used instead.

1.2 Magnetogram preprocessing

For each data sequence, we first disqualify the ineligible images, and divide the values of the magnetograms' pixels by a cosine factor to compensate for the difference between the magnetogram line-of-sight and the local vertical at the solar surface. We designate a reference image in which the sunspot is located near the solar prime meridian, and derotate the magnetograms to remove solar proper motion. Then, we smooth out short-term fluctuations in the time series by computing its five-term cen-

tral moving average. The nonmeaningful irregularities caused by p-mode oscillation are reduced by a factor of $\sqrt{5}$. The frames are cropped to a sunspot-centered field-of-view (FOV) so that the amount of data is reduced while no tracked objects traverse out of the FOV. This completes the preprocessing of magnetograms. Table 1 lists the time intervals of the data sequences, the evolution phases of the sunspots, and some other basic qualities of the data sets.

1.3 Identifying MMFs

We use an automated algorithm introduced in refs. [25–29] to identify and track MMFs. The trajectories of MMFs are pursued by connecting the flux centers of the unipolar magnetic concentrations on adjacent frames.

Many MMFs spend their entire lifetime within the moat and follow penumbral filaments. Some MMFs are observed to cross the inner or outer moat boundaries[21,23]. The moat radius is approximately twice of the penumbra radius[18]. In order to reduce the amount of computation, we demarcate an annular region in which the detecting of MMFs is performed. The inner radius of the annulus is inside the penumbra and the outer radius is outside of the moat, as shown in Figure 1(a). The annulus is thicker than the moat and thus covers

Table 1 Basic properties of all studied sunspot data sets[a)]

NOAA AR	Date	Time interval	Location	Type	Evolution phase	Polarity	Duration (min)	Radius (Mn)	Flux (10^{20} Mx)
08932	2000 Apr	01/10:08-01/18:24	S14W03	β/α	stable, decaying 02nd	−	496	8.9	12.8
08935	2000 Apr	01/10:08-01/18:24	S07W02	β/β	stable, decaying 04th	−	496	13.9	31.3
08971	2000 Apr	28/07:04-28/14:21	N18W20	β/β	stable, large	−	467	22.8	105.0
09147	2000 Sep	01/19:36-02/06:32	N05E17	β/α	stable, inactive	+	656	12.3	23.5
09219	2000 Nov	06/19:53-07/03:47	N06E02	α/α	stable, trailing plage	+	474	12.1	32.2
09267	2000 Dec	14/14:08-14/21:51	N07W01	$\beta\gamma/\beta\gamma$	growing, active, decaying 15th	+	463	14.2	35.3
09335	2001 Feb	07/14:50-08/02:46	N09E14	$\beta\gamma/\beta\gamma$	stable, decaying 09th	+	716	8.0	10.3
09360	2001 Feb	25/10:38-25/23:15	S10E03	α/α	stable, decaying 26th	−	756	6.0	5.6
09493	2001 Jun	12/06:25-12/15:38	N06W02	β/β	decaying 13th	+	552	11.1	20.1
09535	2001 Jul	16/16:25-17/02:57	N06W03	α/α	stable round leading	+	632	12.6	28.8
09575	2001 Aug	17/18:11-18/06:28	N12W02	β/β	stable, decaying 21st	+	737	11.0	25.3
10001	2002 Jun	19/07:30-19/19:36	N20W04	β/β	slowly decaying	+	725	13.8	32.6
10005	2002 Jun	22/00:20-22/11:44	N13W03	β/γ	stable, emerging flux 21st	+	683	13.3	31.8
10162	2002 Oct	24/20:28-25/03:57	N26W03	$\beta\gamma\delta/\beta\gamma\delta$	growing, small field mixing	+	449	19.9	73.0
10171	2002 Oct	31/15:00-01/05:23	N10W15	α/α	decaying	+	863	7.8	7.8
10175	2002 Nov	03/19:49-04/05:38	N14W10	β/β	stable, decaying 07th	−	589	6.3	4.9
10175	2002 Nov	03/07:17-03/14:28	N15W23	β/β	stable, decaying 07th	+	430	10.2	17.9
10176	2002 Nov	03/19:49-04/05:38	N10W03	β/α	stable	+	589	12.8	28.3
10296	2003 Mar	06/12:45-06/18:23	N11W06	$\beta\gamma/\beta\gamma$	stable, decaying 08th	+	338	20.8	70.0
10330	2003 Apr	09/14:07-10/00:48	N07W04	$\beta\gamma/\beta$	stable, leading, decaying 13th	+	641	20.3	75.1
10351	2003 May	06/18:59-07/04:39	N08W02	α/α	stable	+	580	14.5	39.4
10405	2003 Jul	17/14:53-17/21:57	S11W13	β/β	stable, simple, decaying 19th	−	424	8.0	9.8
10421	2003 Aug	03/00:08-03/07:43	S08W13	β/β	slowly decaying	−	455	11.3	22.4
10425	2003 Aug	07/23:53-08/08:18	S09W04	β/β	growing beta region	−	505	12.0	22.9
10606	2004 May	14/06:08-14/13:49	S09W13	β/α	stable, leading	−	461	15.4	38.1
10615	2004 May	22/09:51-23/03:57	N17W15	α/α	stable, decaying 24th	+	1086	11.5	19.8

a) The *time interval* and *duration* show the period of the consecutive data sequence containing few blank and ineligible images. The *evolution phase* was recorded by Big Bear Solar Observatory Active Region Monitor[34] and BBSO Solar Activity Reports. The *flux* is the average sunspot flux within the data sequence.

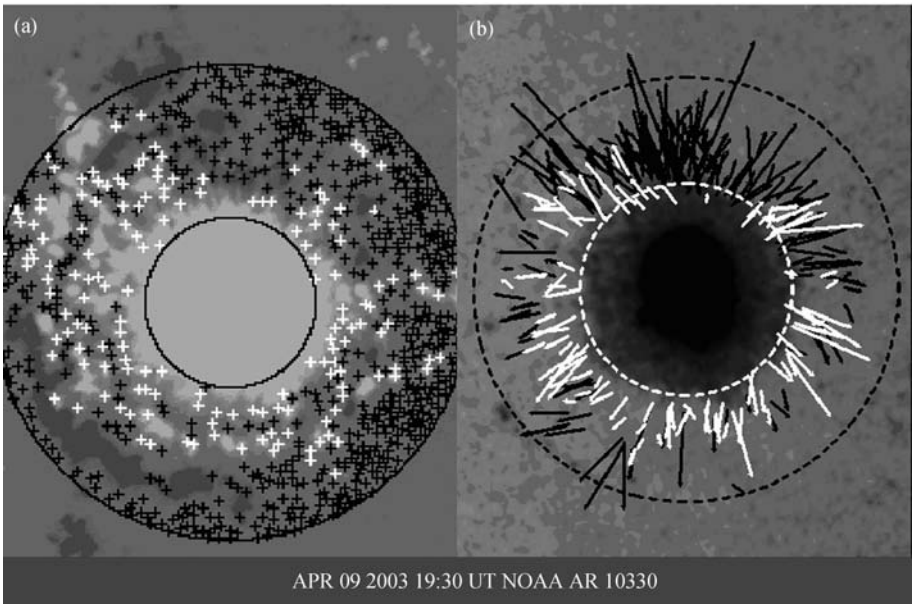

Figure 1 (a) In this five-term averaged magnetogram of NOAA active region 10330, the method finds hundreds of positive and negative polar points (white and black crosses). The two black circles show the designated annulus in which the searching of polar points was performed. (b) The velocity vectors of all the 189 negative and 102 positive MMFs that the program identified over a 10-hour data sequence of AR 10330, superimposed upon a filtergram. The white and black circles show the approximate boundaries of the penumbra and the moat.

the tracks of all possible MMFs. The umbra and the region far outside of the moat are excluded from calculation.

The center and boundary of a sunspot can be used as references to determine the locations of the MMFs relative to the sunspot. In the sunspot area we establish a polar coordinate and define the sunspot's centroid as the pole. On the first and last frame of each filtergram sequence, we manually delineate the visible sunspot boundaries and calculate their least-squares fitting ellipses. Then, on each frame, we set up a boundary ellipse under the assumption that the changes in the boundary ellipse's semimajor, rotation angle, eccentricity, and the center coordinates are all linear within the data time sequence. For the convenience of calculation, these ellipses are employed as the sunspot boundaries to determine the relative positions of the MMFs.

On the magnetograms, the area of MMFs is of the order of magnitude of 1.0 Mm^2. Their flux densities are usually weaker than those of the sunspot boundaries ($\sim$300 G) and higher than the background noise ($\sim$20 G). The flux center of a MMF should be a Gaussian convex core. Using the algorithm described in ref. [25], within the designated circular area, our program calculates the local curvature of each local maxima or minima and tags those pixels that have negative second derivatives. These Gaussian centroids are called "polar points". Figure 1(a) shows the hundreds of polar points found in a magnetogram frame.

The algorithm finds all the possible connections among polar points on neighboring magnetograms. For each polar point on a frame, the method tries to locate and connect its antecedent and successor in the adjacent frames by looking for polar points that have similar fluxes and overlapping spatial locations. The size of the tracking box[26] is 3×3 pixels. These connections as magnetic *objects* on magnetograms are potential candidates for MMFs.

The majority of these numerous magnetic objects are small, weak, and short-time scale flux enhancements. They emerge and disappear transiently and are barely visible to human eye on magnetogram movies. In order to select MMFs

out of these objects, several criteria are applied on their motion and magnetism. These thresholds, as listed in Table 2, were first proposed by Hagenaar et al.[25,27] based on previous observations. We adjusted them by studying the sample pool of moving objects that could be located when stricter or looser criteria were applied. These thresholds screen out a substantial amount of small, short-timescale, flat, weak, and stationary objects. We try to select those objects that can be visually confirmed as MMFs. Figure 1(b) shows the velocities of the MMFs that the algorithm locates on a 10-hour time series of NOAA active region 10330. The movements of two typical MMFs are shown in Figure 2.

Unfortunately, due to the complexity of the moat region, we do not discover a set of reliable and solid criteria to distinguish bipolar and unipolar MMFs. Therefore, in this research bipolarity is not taken into consideration and all MMFs are treated as unipolar.

1.4 Measured quantities

We assume that the distribution of a magnetic object's flux density B is approximately a two-dimensional circular Gaussian function. In a cylindric coordinate, this distribution can be expressed as

$$B(r) = B^{\mathrm{c}} \cdot \exp\left(-\frac{r^2}{2\sigma^2}\right),$$

where r is the distance to the center of the peak, B^{c} is the flux density of the flux center, and σ is the variance of $B(r)$. The area of an object is gauged using FWHM (full width at half maximum) method. The radius r_{o} is considered to be the radius of the peak-centered circle at which the average value of $B(r)$ is equal to half of its amplitude B^{c}. The area is therefore given by $A = \pi r_{\mathrm{o}}^2$. The

Table 2 Criteria for selecting MMFs[a)]

No.	Physical quantities	Criteria	Magnetic objects to be filtered
1	lifetime	$T \geqslant 15$ min	short-timescale emergences
2	distance traveled	$S \geqslant 2.0$ Mm	move less than 3 arcsec
3	average area	$7 \geqslant A_{\mathrm{av}} \geqslant 1$ Mm^2	too big or too small objects
4	speed	$10 \geqslant V \geqslant 0.2$ km/s	stationary objects
5	initial distance to sunspot limb	$D_{\mathrm{ini}} \lesssim (R_{\mathrm{moat}} - R_{\mathrm{spot}})$	emerge outside of moat
6	final distance to sunspot limb	$D_{\mathrm{fnl}} \gtrsim 2$ Mm	vanish too close to penumbra
7	maximum center flux density	$\lvert B^{\mathrm{c}}_{\mathrm{max}}\rvert \geqslant 55$ Gs	too weak objects
8	average center flux density	$\lvert B^{\mathrm{c}}_{\mathrm{av}}\rvert \geqslant 35$ Gs	
9	deviation angle	$\theta \leqslant 45^\circ$	do not move outward
10	the objects that appear at the first/last frame of a data sequence are discarded, because their trajectories have been truncated by the ends of the data sequence.		

a) The definitions of these physical quantities are introduced in sec. 1.4.

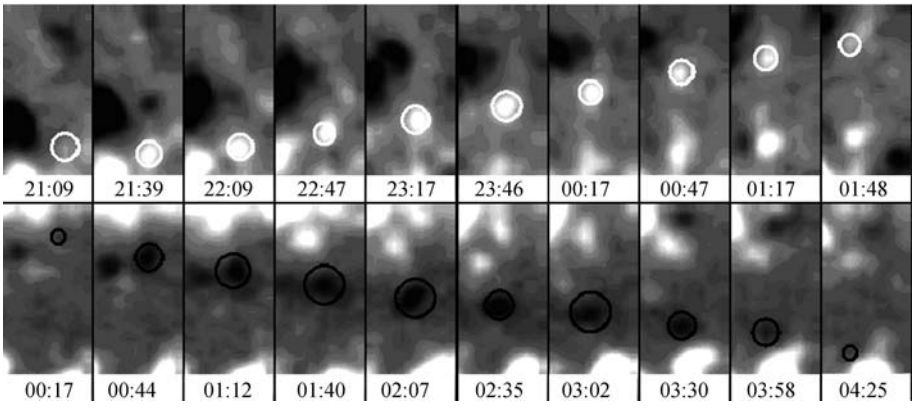

Figure 2 Time series of two typical MMFs moving away from the parent sunspots. The boundaries of their FWHM areas are circled.

radius is related to the variance according to $r_{\rm o} = \sqrt{2\ln 2}\cdot\sigma$. The flux of the object, $\phi(t)$, is defined as the integral of $B(r)$ over $(0, \gamma r_{\rm o})$ and we set $\gamma = 2$.

$$\begin{aligned}\phi(t) &= \int_0^{2\pi}\int_0^{\gamma r_{\rm o}} B(r)\cdot r{\rm d}r{\rm d}\omega \\ &= 2\pi B^{\rm c}\int_0^{\gamma r_{\rm o}} \exp\left(-\frac{r^2}{2\sigma^2}\right)\cdot r{\rm d}r \\ &= \left(\frac{1-2^{-\gamma^2}}{\ln 2}\right)\cdot(\pi r_{\rm o}^2)\cdot B^{\rm c} \\ &\approx 1.3525A\cdot B^{\rm c}.\end{aligned}$$

Therefore, the flux of a magnetic object can be obtained as the product of the object's area A and its center flux density $B^{\rm c}$ as well as a constant scaling factor 1.3525. We denote the maximum value of $\phi(t)$ over the object's lifetime as ϕ.

The flux of a sunspot, $\Phi_{\rm spot}(t)$, is measured by integrating the flux density within the sunspot boundary in each magnetogram frame. $\Phi_{\rm spot}$ represents its average value. The radius of a sunspot, $R_{\rm spot}$, is the average of the semimajor and semiminor of its boundary ellipse. The moat radius $R_{\rm moat}$ is defined in a similar way.

The physical quantities in Table 2 are defined as the following. Lifetime T is the time duration between the first and last appearances of an object. Distance Traveled S is the length of the displacement of an object during its lifetime. Average Area $A_{\rm av}$ is the arithmetic mean of an object's area A over its lifetime. Speed V is the distance traveled by an object divided by its lifetime ($V = S/T$). The upper limit is set according to the maximum speed recorded in literature. Initial/Final Distance to the Sunspot Limb $(D_{\rm ini}, D_{\rm fnl})$ is the distance between the location of the first/last appearance of an object and the sunspot boundary ellipse. These two criteria are adjusted manually by observing the magnetogram movies and outlining an elliptical zone in which MMFs are active. Maximum Center Flux Density $B^{\rm c}_{\rm max}$ is the maximum value of an object's $B^{\rm c}$ during its lifetime. Average Center Flux Density $B^{\rm c}_{\rm av}$ is the mean of an object's $B^{\rm c}$ within its lifetime. Deviation Angle θ is the angle between an object's displacement and the radial direction with respect to the sunspot center.

2 Preliminary results

2.1 Statistics

We differentiate MMFs into two categories by their polarities:

α-MMF: having the polarity opposite to the parent sunspot,

β-MMF: sharing the parent sunspot's polarity. The whole MMF population is separated into $2\times n_{\rm spot}$ subpopulations. $n_{\rm spot}$ is the total number of sunspots, in our research $n_{\rm spot} = 26$. The MMFs in each subset have the same type and parent sunspot. A statistical study is performed in the MMF sample pool to reveal the properties of the two types of MMFs and their relationship with the parent sunspots.

For each identified MMF, several physical quantities (c.f. sec. 1.4) about its motion and magnetism are computed and cataloged. The value of a physical quantity measured from a particular MMF is denoted by the symbol X^{τ}_{si}. X is the physical quantity of interest, e.g. speed, flux. The indices are:

τ is the nominal category specifying the type of the MMF, $\tau \in \{\alpha, \beta\}$.

s is the index of the parent sunspot, $s \in \{1, 2, \cdots, n_{\rm spot}\}$.

i is the index of the MMF, $i \in \{1, 2, \cdots, N(\tau, s)\}$.

$N(\tau, s)$ is the total number of type τ MMFs on sunspot s.

So, X^{τ}_{si} stands for the value of quantity X measured from type τ MMF number i on sunspot s. For each MMF subpopulation, we calculate the central tendencies of the measured quantities. Since many of these quantities' frequency distributions are right-skewed and there is a significant divergence between median and mean, in many cases we use median as the central tendency. The dispersion is measured by interquartile range or standard deviation.

For all of the type τ MMFs around sunspot s, the median value of their X is:

$$\widetilde{X^{\tau}_{s}} = {\rm median}\{X^{\tau}_{si}\}, \quad i = 1, 2, \cdots, N(\tau, s),$$

in which τ and s specify the type and sunspot of the MMF subpopulation. For instance, $\widetilde{\phi^{\alpha}_{s}}$ stands

for the median of the maximum fluxes of all the α-MMFs on sunspot s. We denote the sequence of $\widetilde{X_s^\tau}$ calculated from the type τ subpopulations as $\widetilde{X^\tau}$.

$$\widetilde{X^\tau} = \{\widetilde{X_s^\tau}\}, \quad s = 1, 2, \cdots, n_{\rm spot}.$$

E.g. $\widetilde{\phi^\alpha}$ is the sequence of $\widetilde{\phi_s^\alpha}$ of all the α subpopulations. We call $\widetilde{X^\alpha}$ and $\widetilde{X^\beta}$ together as the *sunspot medians*, $\widetilde{X} = \{\widetilde{X^\alpha}, \widetilde{X^\beta}\}$.

The properties of MMFs of different sunspots are different. In order to investigate the relationship between the sunspots and the characters of the subpopulations of MMFs around them, we plot the sunspot medians ($\widetilde{X}$) of the measured quantities as the functions of the sunspot radii ($R_{\rm spot}$) or flux ($\Phi_{\rm spot}$). For instance, Figure 3(a) shows $\widetilde{T}$, the sunspot medians of MMFs' lifetimes, as a function of $R_{\rm spot}$.

The MMF population as a whole can be described by the frequencies and central tendencies of the measured quantities. The frequency distribution of a quantity can be illustrated by plotting a histogram of the values measured from the entire MMF sample pool. For instance, Figure 3(b) shows the frequency distribution of speed V of all identified α- and β-MMFs. Because the subpopulations $N(\tau, s)$ of MMFs on different sunspots can be different by one order of magnitude, the overall population median or mean of all the X_{si}^τ in the sample pool would be heavily biased by those sunspots that produce more MMFs. In order to give every sunspot *equal weight* on the overall central tendency, we define the *equal-weight population average* $\langle X^\tau \rangle$ of all the type τ MMFs' X as the arithmetic mean of the sunspot median values $\widetilde{X^\tau}$.

$$\langle X^\tau \rangle = {\rm mean}\{\widetilde{X_s^\tau}\} \quad s = 1, 2, \cdots, n_{\rm spot}.$$

In this way, a big sunspot that has hundreds of MMFs would have equal weight on these population averages as that of a small sunspot which only has dozens of MMFs. In the rest of this paper, we use $\langle X^\alpha \rangle$ and $\langle X^\beta \rangle$ as the central tendency of the whole MMF sample pool and refer to them as *population averages*.

The relationships among MMFs' physical properties can be studied by multiple regression. For example, Figure 4 is a scatter diagram of MMFs' initial distances to sunspot ($D_{\rm ini}$, baseline) against their maximum fluxes (ϕ, vertical axis).

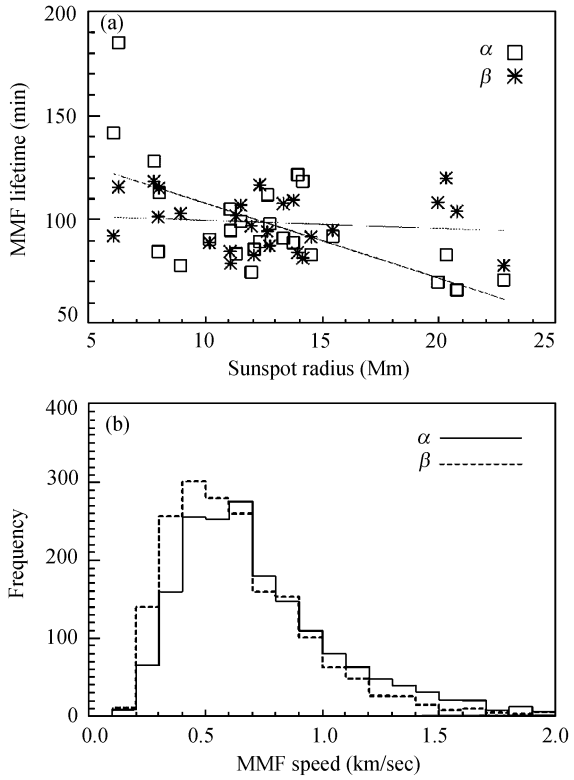

Figure 3 (a) The sunspot median values of MMF's lifetime (T) as a function of sunspot radii. The ordinate of each square/star is the median value of the lifetimes ($\widetilde{T}$) of all the α/β-MMFs found around a particular sunspot, as defined in sec. 2.1. The abscissa is the radius ($R_{\rm spot}$) of the parent sunspots in million meters. The $\widetilde{T}$ of α-MMFs (square) decrease with $R_{\rm spot}$, while those of β-MMFs (star) do not show obvious correlation with $R_{\rm spot}$, as illustrated by the estimated regression lines. The population average lifetime ($\langle T \rangle$, c.f. sec. 3.1) of α/β-MMFs is 1.5/1.7 hours. In general, β-MMFs live slightly longer than α-MMFs. (b) The frequency distribution of all identified MMFs' speeds. The average value $\langle V \rangle$ is about 0.6 km/s. The threshold value for speed is set as 0.2 km/s.

2.2 Population and production

MMFs are found around all studied sunspots, including those not decaying and those not having a penumbra. The *MMF production rate ($R_{\rm prod}$)* of a sunspot is the number of newly emerged MMFs around the sunspot per hour, i.e. the total number of identified MMFs divided by the time duration of

the data sequence. Because criterion No. 10 discards all the MMFs identified in the beginning or at the end of the data set, one median lifetime $\widetilde{T}_s^{\tau}$ is subtracted from the divisor. The *type ratio*,

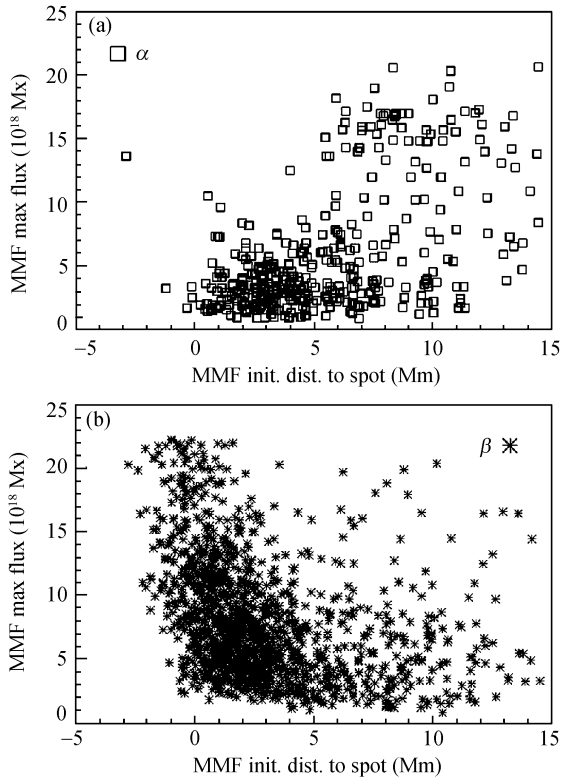

Figure 4 The scatter plots of the maximum fluxes (ϕ) of all the α-MMFs (square) and β-MMFs (star) against their initial distances to the sunspot limb ($D_{\rm ini}$). Majority of the MMFs emerge 0∼5 Mm outside the sunspot limb and have ϕ smaller than 10×10^{18} Mx. Strong α-MMFs usually emerge far from the sunspots, while most strong β-MMFs emerge close or even inside the penumbra boundary.

$R_{\rm type}$, is the quotient of the production rate of α-MMFs divided by that of β-MMFs, $R_{\rm type}$=$R^{\alpha}_{\rm prod}/R^{\beta}_{\rm prod}$. If a sunspot produces equal numbers of α- and β-MMFs, then $R_{\rm type}$ would be 1.

Around the 26 sunspots, the program identifies 3675 MMFs, among which the number of α-MMFs is similar to β-MMFs. $R_{\rm prod}$ varies from 4 to 27 and it increases with the sunspot radius, as shown in Figure 5(a). Large sunspots are more productive in generating MMFs. The four largest sunspots produce more α-MMFs than β-MMFs, while the $R_{\rm type}$ of the five smallest sunspots are less than 1. The $R_{\rm type}$ of middle-sized sunspots scatters. For our limited samples of sunspots, $R_{\rm type}$ varies within the range of 0.2 and 6 and it does not show obvious relationship with the polarity or evolution phase of the parent sunspot.

Figures 4(a) and 4(b) are the scatter plots of ϕ versus $D_{\rm ini}$ (MMFs' initial distances to sunspot limbs) for the α- and β-MMFs respectively. Most of the MMFs emerge at 0−5 Mm outside of the sunspot limb. On average, α-MMFs emerge and disappear farther (4.1/8.3 Mm) away from the parent sunspots than β-MMFs do (2.0/5.5 Mm). There are a certain number of β-MMFs with negative $D_{\rm ini}$. That is to say they are produced inside the penumbra boundary[21,23]. Few α-MMFs emerge within the penumbra.

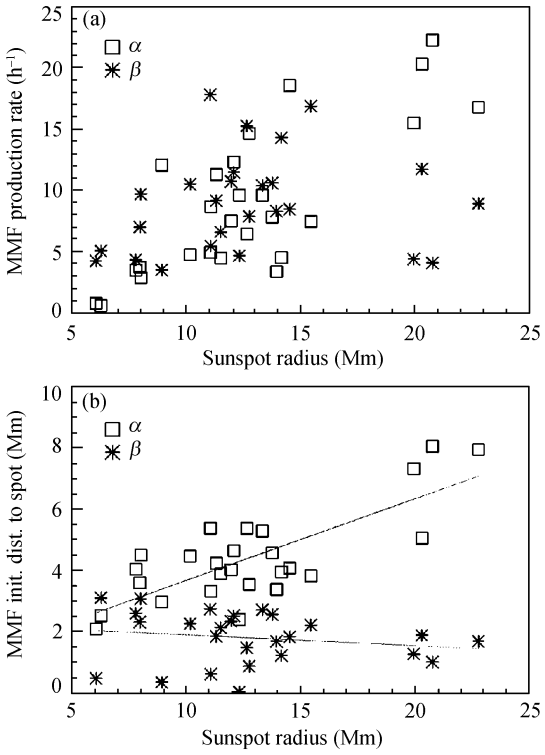

Figure 5 (a) The number of MMFs identified around the sunspots per hour ($R_{\rm prod}$, the MMF production rate) as a function of the sunspot radius. $R^{\alpha}_{\rm prod}$ (square) and $R^{\beta}_{\rm prod}$ (star) increase with $R_{\rm spot}$. (b) The sunspot medians of MMFs' initial distances to the sunspot limbs ($\widetilde{D_{\rm ini}}$) as functions of $R_{\rm spot}$. $\widetilde{D^{\alpha}_{\rm ini}}$ increases with $R_{\rm spot}$ while the distribution of $\widetilde{D^{\beta}_{\rm ini}}$ is narrower and almost sunspot-independent. The plot of the MMFs' final distances to the sunspots ($\widetilde{D_{\rm fnl}}$) has a similar pattern.

Figure 5(b) shows the sunspot medians of $\widetilde{D_{\rm ini}}$ as a function of $R_{\rm spot}$. The plot of the *final* distances to sunspots ($\widetilde{D_{\rm fnl}}$) has a similar pattern. Both $\widetilde{D_{\rm ini}}$ and $\widetilde{D_{\rm fnl}}$ of α-MMFs increase with $R_{\rm spot}$. However, those of β-MMFs do not show such a disposition.

2.3 Motion

Most of the MMFs materialize right outside of the penumbra limb (c.f. Figure 4), then move outward roughly along the radial direction (c.f. Figure 1(b)), and at last vanish somewhere within the moat. A small number of them move into the surrounding network.

During their whole lifetimes, MMFs move 2−12.5 Mm. Figure 6(a) shows the nearly exponential frequency distribution of MMFs' distance traveled (S). The high skewness (1.64) indicates that the S of most MMFs is below the population mean value (3.7 Mm). Figure 6(a) also suggests that numerous objects that move less than 2.0 Mm are discarded by the criterion No. 2. The radial and azimuthal components of MMFs' displacements are also exponentially distributed. $\widetilde{S}^{\alpha}$ ($\widetilde{S}^{\beta}$) is in the range 2.7–5.9 (2.8–3.6) Mm. On average, MMFs move 3.1 Mm in the radial and 0.8 Mm in the azimuthal direction. α-MMFs move a little further than β-MMFs and their deviation angles are approximately 20% larger than those of β-MMFs.

Figure 6(b) shows the sunspot medians of the radial distance traveled ($\widetilde{S_{\rm rad}}$) by MMFs as a function of $R_{\rm spot}$. It shows that $\widetilde{S^{\alpha}_{\rm rad}}$ ranges from 2.5 to 4.5 Mm and it decreases with $R_{\rm spot}$. The α-MMFs of small sunspots move further in the radial direction than those of large sunspots. $\widetilde{S^{\beta}_{\rm rad}}$ is distributed within a small range (2.5–3.4 Mm) and does not show obvious correlation with $R_{\rm spot}$. In the azimuthal direction, the distributions of the traveled distances of both types of MMFs are almost not associated with $R_{\rm spot}$.

Figure 3(b) is a histogram of MMF's speed. 80% of MMFs move at 0.3−1.0 km/s. The population average speed $\langle V\rangle$ is about 0.6 km/s. The fastest ones move at 2.6 km/s. The low-end cutoff is caused by the criterion No. 4. In both radial and azimuthal directions, α-MMFs move about 15% faster than β-MMFs. $\widetilde{V}$ ranges within 0.4–0.9 km/s and does not show obvious correlation with $R_{\rm spot}$ or developing phase.

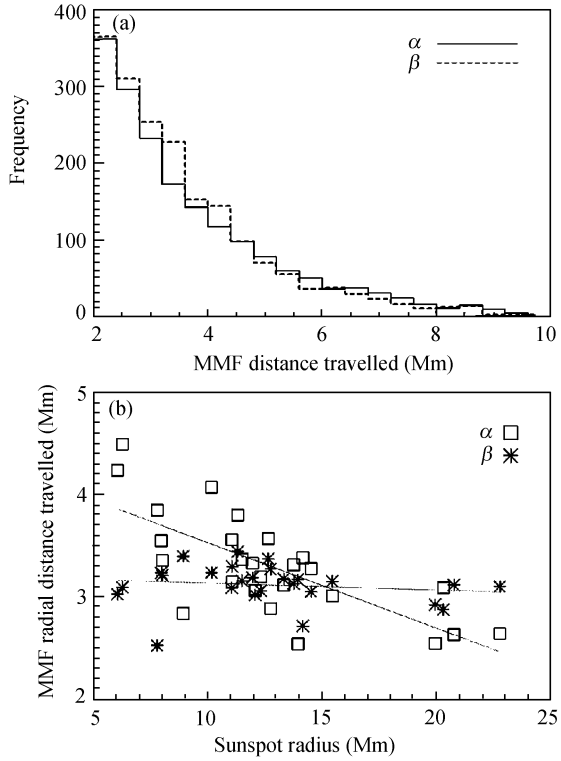

Figure 6 (a) The frequency distribution of all identified MMFs' distance traveled. The nearly-exponential distribution suggests that the majority of MMFs move a relatively short distance. A large number of objects that move a distance shorter than 2 Mm are discarded by our criteria. (b) The sunspot medians of the MMF's radial distance traveled ($\widetilde{S_{\rm rad}}$) as a function of $R_{\rm spot}$. $\widetilde{S^{\alpha}_{\rm rad}}$ (*square*) decrease with $R_{\rm spot}$ while $\widetilde{S^{\beta}_{\rm rad}}$ (*star*) only have a small variation.

On average, the lifetime of α/β-MMFs is ∼1.5/1.7 h. 85% of MMFs live for 0.25−3 h and 2% live longer than 5 h. The longest lifetime of observed α/β-MMFs is 8.4/8.2 h. Figure 3(a) shows that $\widetilde{T^{\alpha}}$ range from 1.1 to 3.1 h and decrease with $R_{\rm spot}$. Small sunspots' α-MMFs usually move further than those of big ones (c.f. Figure 6(b)), which is due to their longer liftimes instead of being able to move faster. The range of $\widetilde{T}^{\beta}$ is narrower (1.3−2.0 h) and they are almost sunspot-independent.

2.4 Magnetic flux content

MMFs appear in a wide range of sizes and fluxes,

which are associated with MMF's type, $D_{\rm ini}$, and $\Phi_{\rm spot}$.

The flux of most of the MMFs is smaller than 10×10^{18} Mx. A comparison of Figures 4(a) and 4(b) shows that, α-MMFs with ϕ larger than 10×10^{18} Mx usually emerge far from the sunspots ($D_{\rm ini}\gtrsim5$ Mm), while most β-MMFs with large fluxes emerge near the sunspot limbs ($D_{\rm ini}\lesssim5$ Mm).

Figures 7(a) and 7(b) are plots of $\widetilde{\phi^\alpha}$ and $\widetilde{\phi^\beta}$ as functions of $\Phi_{\rm spot}$. It shows that large sunspots produce MMFs with large flux. This trend is especially obvious for α-MMFs. The biggest $\widetilde{\phi^\alpha}$ (12.5×10^{18} Mx) is one order of magnitude larger than that of the smallest sunspot (1.6×10^{18} Mx). $\widetilde{\phi^\beta}$ has a smaller range ($4.8\sim11.4\times10^{18}$ Mx) and increases with $\Phi_{\rm spot}$ at a lower rate. For most of the small and middle-sized sunspots, $\widetilde{\phi^\beta}$ is generally larger than $\widetilde{\phi^\alpha}$. These dispositions of $\widetilde{\phi}$ are further illustrated by Figure 8(a), a scatter plot of the sunspot medians of $B^{\rm c}_{\rm av}$ (MMFs' average central flux density) as a function of $\Phi_{\rm spot}$. $\widetilde{B^{\rm c}_{\rm av}}$, esp. α-MMFs', increase with $\Phi_{\rm spot}$. For most of the sunspots, β-MMFs' $\widetilde{B^{\rm c}_{\rm av}}$ is larger than its α counterpart.

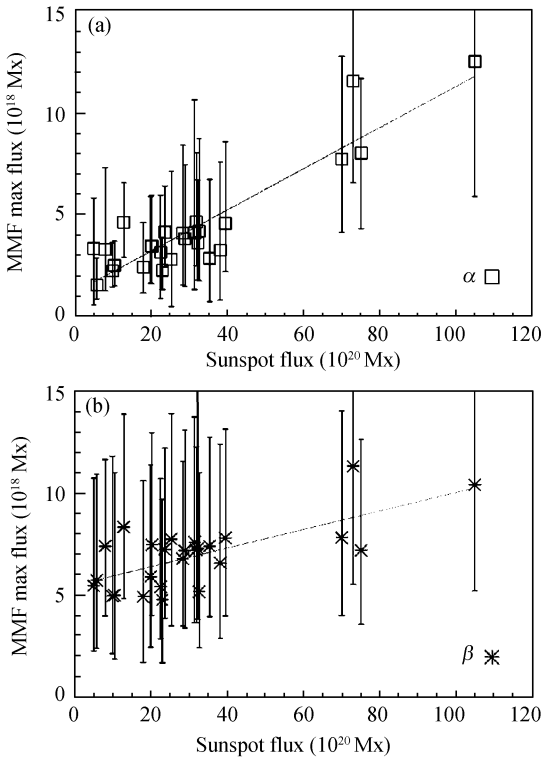

Figure 7 $\widetilde{\phi^\alpha}$ (a) and $\widetilde{\phi^\beta}$ (b) as functions of the sunspot flux. ϕ is MMF's maximum flux. Error bars show the standard deviations. Large sunspots generate MMFs with large flux, especially for type α. MMF's center flux density shows a similar trend (c.f. Figure 7(a)).

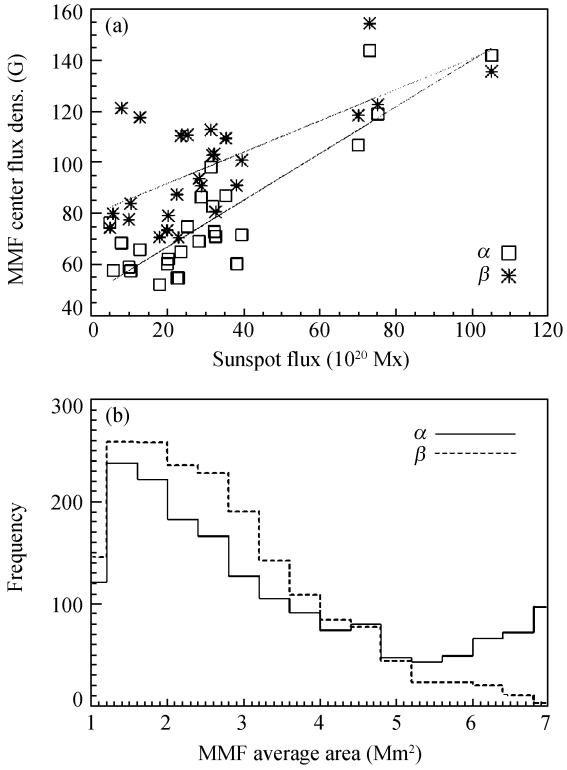

Figure 8 (a) $\widetilde{B^{\rm c}_{\rm av}}$ as a function of $\Phi_{\rm spot}$. $B^{\rm c}_{\rm av}$ is the average flux density of MMF's flux center during the MMF's lifetime. Generally $\widetilde{B^{\rm c}_{\rm av}}$ increase with $\Phi_{\rm spot}$. For most of the sunspots, $\widetilde{B^{\rm c}_{\rm av}}$ of β-MMFs are stronger than those of α-MMFs. (b) The frequency distribution of all identified MMFs' average area $A_{\rm av}$. The upper and lower end cut-offs are set by our criterion No. 3. A large number of small or flat features are discarded.

The sunspot medians of α-MMFs' average area ($\widetilde{A^\alpha_{\rm av}}$) range from 1.1 to 6.6 Mm^2 and increase with $\Phi_{\rm spot}$. The range of $\widetilde{A^\beta_{\rm av}}$ is much narrower (1.4–3.6 Mm^2) and they do not show correlation with $\Phi_{\rm spot}$. The population average value $\langle A_{\rm av}\rangle$ is $\sim$2.3 Mm^2. Figure 8(b) is a frequency histogram of $A_{\rm av}$. Its high skewness indicates that there should be numerous magnetic objects that are smaller than 1 Mm^2 and are screened by our criterion No. 3.

2.5 Sunspot magnetic flux outflow

The relationships among the sunspots' magnetic flux outflow, flux loss, and developing phases are investigated as well.

We calculate the average sunspot *flux loss rate*

$(-\mathrm{d}(\Phi_{\mathrm{spot}}(t))/\mathrm{d}(t))$ using a line-fit routine. We regard the *flux transport rate* as the total flux carried away by MMFs per hour. Within the moat region, a thin elliptical loop concentric to the sunspot boundary is set up to count the traversing MMFs. The size and thickness of the loop are optimized to allow the maximum number of MMFs to cross its inner or outer boarder. The flux transport rate is the total flux of these traversers per hour: $|\sum^{\mathrm{cross}}\phi|$.

Although our measurements of flux transport rate ($0.2-8.3\times10^{19}$ Mx·h^{-1}) basically comports with the range of other observations, they do not show noticeable correlation with the sunspot flux loss rates. For some of the sunspots, neither the flux transport rate nor the flux loss rate is consistent with the recorded developing phases.

3 Conclusion

We develop a tracking code and use it to pursue MMFs on the magnetogram series of 26 sunspots. A statistical analysis on the kinematic and magnetic properties of the identified MMFs is carried out. We find that the statistical characteristic of a sunspot's MMF set is relevant to the parent sunspot. In several aspects the two categories of MMFs have different statistical characteristics.

We find that the sunspots produce 4 to 27 MMFs per hour and this production rate tends to increase with the sunspot radius. Generally, α-MMFs emerge and disappear farther from the sunspot boundary than β-MMFs do. This is especially obvious for MMFs with above-average flux. α-MMF's initial/final distances to the sunspot limbs increase with the parent sunspot radius. β-MMFs emerge/vanish at similar distances among the sunspots.

The α- and β-MMF subpopulations exhibit a wide range of central tendencies. According to the *sunspot median* values, typical α/β-MMFs emerge at $2.2-8.1/0.1-3.2$ Mm outside the penumbra limb. They are $1.1-6.6/1.4-3.6$ Mm^2 in area and carry $1.4-12.5/4.8-11.4$ $\times10^{18}$ Mx of flux. They live for $1.1-3.1/1.3-2.0$ h, and travel a distance of $2.7-5.9/2.8-3.6$ Mm with the speed of $0.5-0.9/0.4-0.7$ km/s. The frequency distributions of the MMFs' distance traveled, flux, and area are approximately exponential, with most of values below the arithmetic mean.

The sunspot median values of α-MMFs' distance traveled and lifetime decrease with the sunspot radius, while those of α-MMFs' area and flux increase with sunspot flux. Compared to α-MMFs of small sunspots, large sunspots tend to produce big α-MMFs that live shorter, move nearer, and carry more flux. It is noticed that, in some of the scatter plots, few outliers bias the least squares estimation. In our future research, residual analysis will be performed to construct the confidence intervals and estimate the regression coefficients properly.

β-MMF's motion and magnetism have much weaker correlations with Φ_{spot} or R_{spot}than α-MMFs do. This might indicate that the generation mechanism of β-MMFs is relatively uniform among different sunspots, while that of α-MMFs is more relevant to the structure and surroundings of the sunspots. This needs to be further studied in the scenario of supergranulation[19] and subphotospheric convection.

We calculate the sunspots' magnetic flux outflow transported by MMFs and the sunspot flux loss, but do not find obvious correlation between them. The nearly exponential distributions of MMF's area, distance traveled, and flux are consistent with Hagenaar's observation[27] and suggest that numerous small, weak, short-timescale objects fall under our criteria and are not counted. These culls might constitute a substantial amount of sunspots' flux outflow. As Vrabec[5] has commented, the magnetic flux outflow is a "considerably more complicated process than" fragmentation of sunspots into MMFs. Further investigations using higher resolution data and estimation methods need to be carried out to estimate the flux outflow.

We plan to examine a larger sample of sunspots to investigate the relationship between the characteristics of MMFs and the parent sunspot more thoroughly. We also intend to continue this study on higher resolution data, and discuss MMFs' evolution and physical structure.

The authors would like to thank Jiangtao Su, Haiqing Xu, Yu Gao, and H. J. Hagenaar for reading and commenting

on the manuscript. Thanks are also due to the referees for their comments and suggestions on how to improve the manuscript. This research has made use of Interactive Data Language, SolarSoft[31]*, SAOImage DS9*[32]*, Linfit*[33] *and MDI High-Resolution Data Catalog. SOHO is a project of international collaboration between ESA and NASA.*

1 Sheeley N R Jr. The evolution of the photospheric network. Sol Phys, 1969, 9: 347–357
2 Vrabec D. Magnetic fields spectroheliograms from the San Fernando observatory. In: Howard R, ed. Sol Magn Fields, IAU Symposium, 1971, 43: 329–339
3 Harvey K, Harvey J. Observations of moving magnetic features near sunspots. Sol Phys, 1973, 28: 61–71
4 Shine R, Title A. Sunspots: Moving magnetic features and moat flow. In: Murdin P, ed. Encyclopedia of Astronomy and Astrophysics, 2001
5 Vrabec D. Streaming magnetic features near sunspots. In: Athay R G, ed. Chromospheric Fine Structure, IAU Symposium, 1974, 56: 201–231
6 Bernasconi P N, Rust D M, Georgoulis M K, et al. Moving dipolar features in an emerging flux region. Sol Phys, 2002, 209: 119–139
7 Zhang J, Solanki S K, Woch J. Discovery of inward moving magnetic enhancements in sunspot penumbrae. Astron Astrophys, 2007, 475: 695–700
8 Wilson P R. The cooling of a sunspot. III: Recent observations. Sol Phys, 1973, 32: 435–439
9 Wilson P R. The generation of magnetic fields in photospheric layers. Sol Phys, 1986, 106: 1–28
10 Spruit H C, Title A M, van Ballegooijen A A. The generation of magnetic fields in photospheric layers. Sol Phys, 1987, 110: 115–128
11 Lee J W. Observational evidence for various models of moving magnetic features. Sol Phys, 1992, 139: 267–273
12 Penn M J, Kuhn J R. Imaging spectropolarimetry of the He I 1083 nanometer line in a flaring solar active region. Astrophys J, 1995, 441: L51–L54
13 Yurchyshyn V B, Wang H, Goode P R. On the correlation between the orientation of moving magnetic features and the large-scale twist of sunspots. Astrophys J, 2001, 550: 470–474
14 Zhang J, Solanki S K, Wang J. On the nature of moving magnetic feature pairs around sunspots. Astron Astrophys, 2003, 399: 755–761
15 Choudhary D P, Balasubramaniam K S. Multiheight properties of moving magnetic features. Astrophys J, 2007, 664: 1228–1233
16 Kubo M, Shimizu T, Tsuneta S. Vector magnetic fields of moving magnetic features and flux removal from a sunspot. Astrophys J, 2007, 659: 812–828
17 Ryutova M, Hagenaar H. Magnetic solitons: Unified mechanism for moving magnetic features. Sol Phys, 2007, 246: 281–294
18 Brickhouse N S, Labonte B J. Mass and energy flow near sunspots. I - observations of moat properties. Sol Phys, 1988, 115: 43–60
19 Wang H. On the relationship between magnetic fields and supergranule velocity fields. Sol Phys, 1988, 117: 343–358
20 Zhang H, Ai G, Wang H, et al. Evolution of magnetic fields and mass flow in a decaying active region. Sol Phys, 1992, 140: 307–316
21 Sainz Dalda A, Martínez Pillet V. Moving magnetic features as prolongation of penumbral filaments. Astrophys J, 2005, 632: 1176–1183
22 Li X, Zhang J, Wang J. Unipolar moving magnetic features: An observation. In: Bothmer V, Hady A A, eds. Solar Activity and its Magnetic Origin, IAU Symposium, 2006, 233: 83–84
23 Ravindra B. Moving magnetic features in and out of penumbral filaments. Sol Phys, 2006, 237: 297–319
24 Brooks D H, Kurokawa H, Berger T E. An Hα surge provoked by moving magnetic features near an emerging flux region. Astrophys J, 2007, 656: 1197–1207
25 Hagenaar H J, Schrijver C J, Title A M, et al. Dispersal of magnetic flux in the quiet solar photosphere. Astrophys J, 1999, 511: 932–944
26 Fletcher L, Pollock J A, Potts H E. Tracking of TRACE ultraviolet flare footpoints. Sol Phys, 2004, 222: 279–298
27 Hagenaar H J, Shine R A. Moving magnetic features around sunspots. Astrophys J, 2005, 635: 659–669
28 DeForest C E, Hagenaar H J, Lamb D A, et al. Solar magnetic tracking. I. Software comparison and recommended practices. Astrophys J, 2007, 666: 576–587
29 Lamb D A, DeForest C E, Hagenaar H J, et al. Solar magnetic tracking. II. The apparent unipolar origin of quiet-sun flux. Astrophys J, 2008, 674: 520–529
30 Scherrer P H, Bogart R S, Bush R I, et al. The solar oscillations investigation - michelson doppler imager. Sol Phys, 1995, 162: 129–188
31 Freeland S L, Handy B N. Data analysis with the solarSoft system. Sol Phys, 1998, 182: 497–500
32 Joye W A. New features of SAOImage DS9. In: Gabriel C, Arviset C, Ponz D, et al., eds. Astronomical Data Analysis Software and Systems XV, ASP Conference Series, 2006, 351: 574–576
33 Wiegelmann T, Inhester B, Lagg A, et al. How to use magnetic field information for coronal loop identification. Sol Phys, 2005, 228: 67–78
34 Gallagher P T, Moon Y J, Wang H. Active-region monitoring and flare forecasting I. Data processing and first results. Sol Phys, 2002, 209: 171–183